ACS OMEGA

http://pubs.acs.org/journal/acsodf

Article

Role of Additives in Electrochemical Deposition of Ternary Metal Oxide Microspheres for Supercapacitor Applications

Avijit Biswal, Prasanna Kumar Panda, Achyuta Nanda Acharya, Subhashree Mohapatra, Nibedita Swain, Bankim Chandra Tripathy, Zhong-Tao Jiang, and Manickam Minakshi Sundaram*

Cite This: *ACS Omega* 2020, 5, 3405−3417

Read Online

ACCESS | Metrics & More | Article Recommendations

ABSTRACT: A simple two-step approach has been employed to synthesize a cobalt−nickel−copper ternary metal oxide, involving electrochemical precipitation/deposition followed by calcination. The ternary metal hydroxide gets precipitated/deposited from a nitrate bath at the cathode in the catholyte chamber of a two-compartment diaphragm cell at room temperature having a pH ≈ 3. The microstructure of the ternary hydroxides was modified in situ by two different surfactants such as cetyltrimethylammonium bromide and dodecyltrimethylammonium bromide in the bath aiming for enhanced storage performance in the electrochemical devices. The effect of the surfactant produces a transition from microspheres to nanosheets, and the effect of micelle concentration produces nanospheres at a higher ion concentration. The ternary hydroxides were calcined at 300 °C to obtain the desired ternary mixed oxide materials as the electrode for hybrid supercapacitors. X-ray diffraction analysis confirmed the formation of the ternary metal oxide product. The scanning electron microscopy images associated with energy-dispersive analysis suggest the formation of a nanostructured porous composite. Ternary metal oxide in the absence and presence of a surfactant served as the cathode and activated carbon served as the anode for supercapacitor application. DTAB-added metal oxide showed 95.1% capacitance retention after 1000 cycles, achieving 188 F/g at a current density of 0.1 A/g, and thereafter stable until 5000 cycles, inferring that more transition metals in the oxide along with suitable surfactants at an appropriate micellar concentration may be better for redox reactions and achieving higher electrical conductivity and smaller charge transfer resistance. The role of various metal cations and surfactants as additives in the electrolytic bath has been discussed.

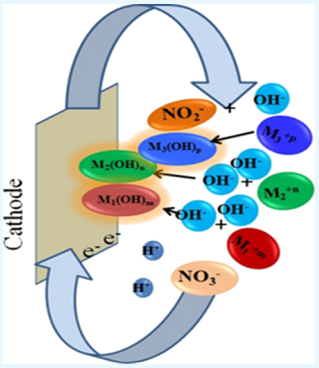

1. INTRODUCTION

In the ever-increasing trend of industrialization, the prevalent demands and applications of electrochemical energy storage devices such as batteries and supercapacitors are unavoidable. Day to day a new quest for an energy material has been showcased that can increase the utility and capacity of the energy storage devices in a more economic and ecofriendly way. The performance of energy storage devices is governed by certain key parameters such as power density, energy density, specific capacitance, and cycle life stability.[1] Typically, supercapacitor electrodes should possess certain key features such as high power, fast charge−discharge kinetics, and long cycle life, making it an attractive and most demanding energy material.[2] Amid the two categories of supercapacitors such as electrical double-layer capacitors (EDLCs) and the faradaic redox reaction pseudocapacitors, the latter one draws much attention as it offers high capacitance and high energy density than the former.[3−9] Asymmetric supercapacitors fall under "faradaic redox pseudocapacitors" which are in high demand because of their wide electrochemical window with high specific capacitance possessing a battery-type behavior, and these key features make them seemly candidates to fulfill the needs of the incipient energy storage applications in the market.[10,11]

The specific capacitance basically depends on the choice of chosen pseudocapacitive behavior in the nature material or the intrinsic behavior of the active material. Hence, the selection of an electrode material should satisfy several parameters including high specific surface area, nanostructured morphology, controlled porosity, enabling the system to have improved specific capacitance, high electronic conductivity, and high power as well as energy density of the capacitor.[2,9]

Various conducting polymers and metal oxide composites are well known candidates for pseudocapacitance behavior that has attracted researcher's attention.[12,13] However, at present, the environmental friendly transition-metal oxides such as NiO, Co_3O_4, and MnO_2 have been found to exhibit superior redox activity with large natural abundance and simplistic and

Received: October 30, 2019
Accepted: January 29, 2020
Published: February 11, 2020

scalable synthesis delivering high capacitance at a relatively low cost than conducting polymers and rare earth oxides. Although Ni, Co, and Mn share common merits, each transition metal oxide differs in their crystal structures and redox behaviors.[14−17] Several limitations such as slow diffusion rate and low electronic conductivities restrain the materials from their high performance for supercapacitor applications.[18] Considering the above drawbacks, binary or ternary metal oxides have been proposed, which offer the synergistic effect of individual metal ions that can ameliorate the capacitive performance with a widened potential window, superior conductivity, and more active sites with improved stability.[19] Several works are carried out on binary metal oxides[20−27] that were found to exhibit excellent electrochemical performance over monometallic transition metal oxides due to multiple oxidation states in the mixed oxide materials.[28−30]

Although several studies have been carried out on binary mixed oxide materials, but only limited works are available on the ternary oxides (TO). Among the reported data, nanostructured Mn−Ni−Co oxide,[31] Mn−Ni−Co TO nanowires,[32] and Zn−Ni−Co TOs[18] show much improved capacitance for supercapacitor applications. On comparing with pure oxide or binary oxides, the TOs showed better performance in terms of cost and specific capacitance. However, a facile electrochemical deposition to synthesize TOs is not widely reported. The synergistic effect consists of high capacity attributed by Ni leading to improved active site density, conductivity, and roughness, while the presence of Co leads to increased electronic conductivity, and the role of Zn is attributed to good electrical conductivity that results in the overall improvement of the capacitance in the energy storage device.[5,7] Furthermore, TOs offer abundant structural defects due to the presence of multiphase metal oxides by several metal ions leading to a stable and improved cycle life.[18] On the other hand, in the field of electrodeposition, it is well known that the nucleation and growth of the crystal structures of the internal active oxide materials can be altered by various structure-directing agents/surfactants such as cetyltrimethylammonium bromide (CTAB), cetyltrimethylammonium chloride (CTAC),[33−35] tetraethylammonium bromide, tetrapropylammonium bromide, tetrabutylammonium bromide,[36] tetradecyltrimethylammonium bromide,[37] sodium lauryl sulphate,[38] and sodium dodecyl sulfate.[38] Therefore, it is imperative to use organic additives as surfactants in the electrolytic bath to improve the structural and morphological properties of the oxide deposits. The outcome of these surfactants revealed that they modified the morphology of the crystals that significantly influenced the storage property when they were tested as an electrode for energy storage devices. Still, several surfactants are unexplored in this field. However, identifying a suitable surfactant for a specific application (like energy storage), one can achieve an improved storage performance. To this end, we have adopted this concept and validated the role of surfactants and the micellar concentration in depositing ternary metal oxides such as cobalt, nickel, and copper as cations.

In this work, using a facile electrochemical approach, ternary metal oxide has been synthesized, and their microstructures are tweaked with in situ addition of surfactants such as CTAB and dodecyl trimethyl ammonium bromide (DTAB) at an appropriate amount. In the literature, the electrochemical synthesis of oxides is predominantly based on the potentiostatic technique, which are suitable for thin film formation or obtaining a product in a small scale. However, to the best of our knowledge, no reported work is yet available on the galvanostatic technique for synthesizing TO materials and its structural modification by an in situ addition of the surfactant in the bath. This approach of electrodeposition can lead to a large-scale production of the requisite material in a more cost-effective and ecofriendly manner, avoiding unwanted reactions.

Owing to excellent advantages offered by ternary metal oxides with the limited research available in this field, an attempt has been made to synthesize cobalt−nickel−copper (Co−Ni−Cu) mixed oxides and modified mixed oxide with surfactants as additives by a novel galvanostatic technique in a two-step route comprising electrodeposition followed by calcination. The Ni and Co oxides possess high redox activity but their capacitance decay could be inevitable because of their phase transformation during cycling. However, the addition of Cu may act as a pillaring effect to stabilize the cycling behavior. To examine this, the obtained TOs are tested as electrodes for supercapacitor applications, and their capacitance is found to be enhanced in the presence of DTAB as an additive at critical micelle concentration (cmc) and above. It has been shown in this work that the obtained specific capacitance value (188 F/g at 0.1 A/g) for the modified ternary metal oxide exceeds the previously reported values for ternary metal oxides,[31,32] which is attributed to the role of additives and CuO.

2. EXPERIMENTAL SECTION

2.1. Preparation of Ternary Metal Hydroxides and Modified Ternary Metal Hydroxides by Electrodeposition. All the chemicals used in the present work were of pure analytical grade and were used as received. Electrodeposition was carried out in a two-compartment diaphragm cell. Current was supplied from a constant current dc source (Aplab) in the galvanostatic mode. Details of the experimental setup was described elsewhere ref 39. Mixed Co−Ni−Cu ternary hydroxides (TH) were deposited from their nitrate bath containing 30 g dm^{-3} $Co(NO_3)_2{\cdot}7H_2O$ + 30 g dm^{-3} Ni $(NO_3)_2{\cdot}7H_2O$ with varying concentrations of Cu $(NO_3)_2{\cdot}3H_2O$ (5, 10, 15 g dm^{-3}) as their respective metal ions. The cathodic reduction of Co^{2+} to $Co(OH)_2$, Ni^{2+} to $Ni(OH)_2$, and Cu^{2+} to $Cu(OH)_2$ were carried out on a stainless steel cathode placed in parallel to an iridium oxide-coated titanium (IrO_2−Ti) anode at a cathodic current density of 200 A m^{-2}.

Modified Co−Ni−Cu hydroxides were synthesized exactly to that of ternary metal hydroxides from a nitrate bath with fixed a electrolyte concentration of 30 g dm^{-3} $Co(NO_3)_2{\cdot}7H_2O$ + 30 g dm^{-3} Ni $(NO_3)_2{\cdot}7H_2O$ + 10 g dm^{-3} Cu $(NO_3)_2{\cdot}3H_2O$ but with varying amounts of two different surfactants, namely, CTAB and DTAB. For cationic surfactants, such as CTAB and DTAB, pH values of the aqueous solutions are 5.6 and 5.5, respectively. Three sets of experiments were carried out for each surfactant. Each surfactant were added as per their cmc, below the cmc, and above the cmc value. The values of the cmc for CTAB and DTAB are 14.4 and 1 mM, respectively. The below and above cmc values for CTAB and DTAB are 0.1, 10 and 1.4, 140 mM, respectively. All the experiments were carried out for 2 h at room temperature. After which the deposited materials were removed from the cathode and washed thoroughly with deionized water before drying in an oven. Subsequently, the dried materials were cooled in a desiccator and subjected to physical tests such as X-ray diffraction (XRD), Fourier-transform Infrared spectroscopy (FT-IR), porosity, and other microscopy analyses.

https://dx.doi.org/10.1021/acsomega.9b03657
ACS Omega 2020, 5, 3405−3417

2.2. Calcination of Hydroxide to Form Oxide and Sample Labelling. THs samples were calcined at 300 °C for 2 h to convert them to their respective oxides. Then, the calcined materials were subjected to physical and electrochemical characterization. Co−Ni−Cu mixed THs deposited from a nitrate bath with a respective concentration ratio of 30:30:10 (g dm^{-3}), and the corresponding oxides obtained after calcination at 300 °C were labeled as TH and TO, respectively.

The modified THs deposited from a mixed bath containing CTAB, DTAB at cmc, below the cmc, and above the cmc are labelled as $THCB_{CMC}$, $THCB_{LCMC}$, $THCB_{HCMC}$, $THDB_{CMC}$, $THDB_{LCMC}$, and $THDB_{HCMC}$. Modified TOs calcined at 300 °C for CTAB and DTAB at cmc, low cmc, and high cmc are labelled as $TOCB_{CMC}$, $TOCB_{LCMC}$, $TOCB_{HCMC}$, $TODB_{CMC}$, $TODB_{LCMC}$, and $TODB_{HCMC}$ respectively.

2.3. Material Characterization. Different physicochemical characterization was carried out to identify the phase, bonding, surface morphology, and chemical composition of the THs and calcined oxide materials. Phase analysis was carried out using a Phillips powder diffractometer (PANanalytical PW 1830) using Cu Kα radiation. FT-IR spectroscopic analyses were carried out by using a Nicolet 6070 spectrophotometer at room temperature. The surface morphology of the samples was determined using scanning electron microscopy (FESEM, ZEISS SUPRA 55) together with energy dispersive analysis. Nitrogen adsorption−desorption studies were carried out using Quantachrome (Autosorb-iQ) surface area and porosity analyzer. Before analyzing, the samples were degassed at 100 °C overnight. Chemical analysis was carried out by an atomic absorption spectrophotometer (AAS) to determine the composition of the synthesized materials.

2.4. Electrochemical Characterization. The electrodeposited oxide materials were coated on a graphite substrate in the area of 1 cm × 1 cm. Graphite was chosen as the substrate because of its low cost and can be used multiple times. The chosen substrate was polished with an emery sheet and thoroughly washed with deionized water and dried before using. The working electrode was prepared by mixing the active material (metal oxide), carbon black, and polyvinylidene fluoride in a 75:15:10 wt % ratio. All ingredients were mixed in *N*-methyl-2-pyrrolidone (250 μL) to make a slurry which was coated on a graphite substrate. The coated electrode was then dried on a hot plate (at 40 °C for an hour) to evaporate the solvent before any electrochemical testing. The mass of the coated sample was determined from the weight difference before and after the coating.

The electrochemical behavior of metal oxide materials was investigated by cyclic voltammetry and impedance spectroscopy using an SP-150, Bio-Logic instrument controlled by EC-Lab software, and galvanostatic charge−discharge and rate capability measurements by using a battery analyzer (MTI corp, USA) operated by a battery testing system. Electrochemical behavior of ternary metal oxides was investigated by using three-electrode cells using 2 M NaOH as an electrolyte, and Pt wire and Hg/HgO were used as the counter and reference electrodes, respectively, over a potential range from 0.0 to 0.6 V at different sweep rates. Galvanostatic charge−discharge in the potential range of 0.2−1.6 V at various current densities. Electrochemical impedance spectroscopy (EIS) was carried out with an amplitude of 5 mV over a frequency range of 0.01 Hz to 100 kHz at open circuit potential. The specific capacitance (C_{sp}), energy density (E_{sp}), and the power density of the device were calculated using the following equations

$$C_{sp} = \frac{It}{\Delta V m} \quad (1)$$

$$E_{sp} = \frac{\frac{1}{2} C_{sp} (\Delta E)^2}{3.6} \quad (2)$$

$$P_{sp} = \frac{E_{sp}}{t} \times 3600 \quad (3)$$

where C_{sp} is the specific capacitance (F g^{-1}), I is the current (A) imposed to the cell for charge−discharge, Δt is the time taken to discharge in seconds (calculated from the discharge curves), m is the weight of the active electrode ($TOCB_{CMC}$, $TOCB_{LCMC}$, $TOCB_{HCMC}$, $TODB_{CMC}$, $TODB_{LCMC}$, and $TODB_{HCMC}$) in grams, and ΔE is the voltage window (E). For a hybrid cell, the two-electrode configuration, activated carbon is used as the anode with TOCB (or) TODB as the cathode within the voltage range of 0.0−1.6 V using 2 M NaOH as an electrolyte. The mass of a typical electrode is between 20 and 25 mg. In order to maintain the charge conservation between the two electrodes, the mass ratio was calculated using eq 4

$$m^+/m^- = (C_{sp-} \times \Delta E -)/(C_{sp+} \times \Delta E +) \quad (4)$$

where m represents the mass in g. C_{sp-} and C_{sp+} represent the specific capacitance for the ac (125 F/g) and metal oxides (525 F/g), respectively (calculated from eq 1). $\Delta E-$ and $\Delta E+$ are the discharge−charge potential range for the ac and TOCB and TODB electrodes, respectively.

3. RESULTS AND DISCUSSION

3.1. Electrodeposition of Ternary Metal Hydroxide. The present synthesis is based on electrochemical deposition.

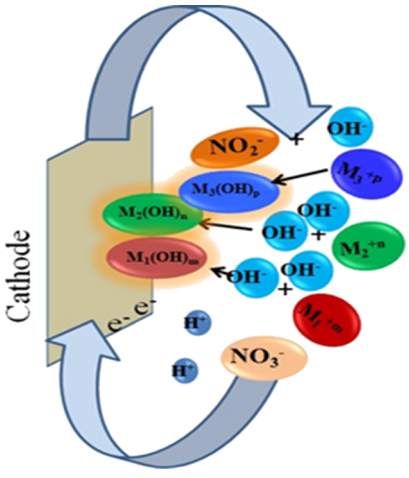

Figure 1. Schematic diagram of the general mechanism of electrochemical precipitation/deposition of TH from nitrate bath.

In this work, nitrate solutions of three transition-metal cations such as Co^{2+}, Ni^{2+}, and Cu^{2+} at different concentrations were taken as electrolytes for the synthesis of mixed TH. All the experiments were carried out at room temperature maintaining the solution pH at 3 at a current density of 200 A m^{-2}. Generally, mixed hydroxide of cobalt and nickel is deposited from their mixed nitrate bath at a solution pH of 4.[39] However,

https://dx.doi.org/10.1021/acsomega.9b03657
ACS Omega 2020, 5, 3405−3417

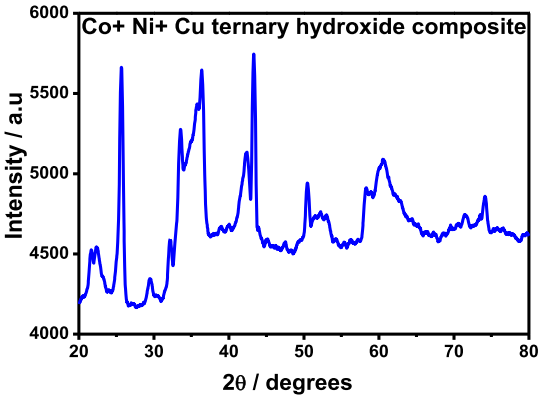

Figure 2. XRD pattern of TH deposited from a nitrate bath containing 30 g dm^{-3} Co + 30 g dm^{-3} Ni and +10 g dm^{-3} Cu.

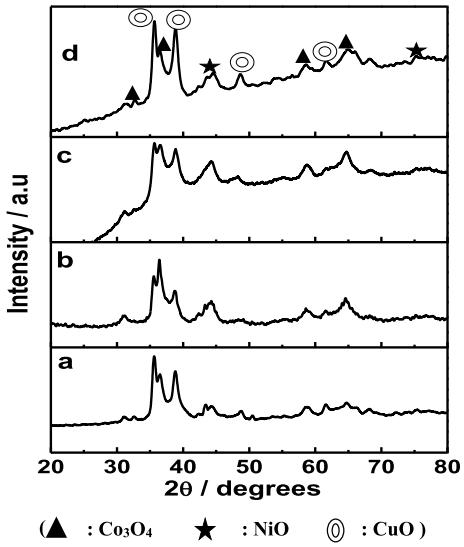

Figure 3. XRD pattern of the calcined form of ternary metal hydroxides (a) TO and modified ternary metal hydroxides (b) $TOCB_{CMC}$, (c) $TODB_{CMC}$, and (d)$TODB_{HCMC}$.

after mixing copper nitrate to the mixed nitrate bath of cobalt and nickel, precipitation starts at pH 4; thus the solution of the ternary metal nitrate electrolyte bath was maintained at pH 3 before taking it for electrodeposition.

During the electrolysis, nitrate ions from the bath play a vital role in the deposition of metal hydroxide such as cobalt hydroxide from cobalt nitrate solution.[40] Initially, when potential is applied to the electrolytic cell, the reduction of nitrate ions take place and hydroxyl ions are formed. The standard reduction potential (E_0) of nitrate ion is −0.31 V versus saturated calomel electrode. The process during reduction is given as

$$NO_3^- + H_2O + 2e^- \rightarrow NO_2^- + 2OH_{(aq)}^- \quad (5)$$

Hydroxyl groups formed via electrochemical reduction are expected to react with M^{2+} ions present in the electrolyte. As a result, cobalt hydroxide is deposited or electrochemically precipitated on the substrate according to the reaction in eq 5

$$Co^{2+} + 2OH^- \rightarrow Co(OH)_2 \quad (6)$$

Nickel and copper hydroxide are also deposited in a similar manner

$$Ni^{2+} + 2OH^- \rightarrow Ni(OH)_2 \quad (7)$$

$$Cu^{2+} + 2OH^- \rightarrow Cu(OH)_2 \quad (8)$$

In general, the cathodic deposition/precipitation mechanism from an electrolyte containing a single metal M with valency m is as follows.

$$M^{m+} + mOH^- \rightarrow M(OH)_m \quad (9)$$

However, if the solution contains multiple metals such as M_1, M_2, and M_3 with valances +m, +n, and +p, respectively, the probable mechanism for electrochemical precipitation/deposition may be as follows.

$$M_1^{+m} + M_2^{+n} + M_3^{+p} + (m + n + p)OH^- \rightarrow M_1M_2M_3(OH)_{m+n+p} \quad (10)$$

The schematic diagram of the probable mechanism of electrochemical precipitation/deposition TH is shown in Figure 1. The electrodeposited THs samples were calcined at 300 °C for 2 h to obtain TOs.

3.2. Physico Chemical Characterization. To verify the obtained electrodeposited Co−Ni−Cu mixed TH and its calcined form, structural elucidation and determination of the surface morphology of the synthesized materials were carried out using XRD, FTIR, and FESEM coupled with EDS and BET analyses. Chemical analysis by an atomic absorption spectrophotometer (AAS) was also carried out to quantify the composition of the material.

3.2.1. XRD Study. Figure 2 shows the XRD pattern of the electrodeposited TH materials from baths containing cobalt nitrate, nickel nitrate, and copper nitrate mixed solution. The diffraction pattern revealed that in all the cases, the composite of ternary mixed hydroxide was obtained. The XRD pattern revealed the formation of mixed phases of $Co(OH)_2$, $Ni(OH)_2$, and $Cu(OH)_2$ with a hexagonal crystal structure, with reference to JCPDS card nos.: 02-0925, 06-0075, 35-0505. Figure 3 shows the mixed TO phases consisting of cobalt, nickel, and copper. The XRD pattern of ternary cobalt−nickel−copper oxide (TO) with diffraction peaks of 32.48, 36.56, 58.49, and 65.05 (JCPDS card no. 80-1537) corresponds to the Co_3O_4 crystal lattice. However, diffraction peaks at about 43.68 and at 75.15 corresponds to the planes of NiO crystal lattices (JCPDS card no. 22-1189), and the peaks at ∼35.57, 39.01, 48.65, and 61.67 corresponds to the planes of CuO (JCPDS card no. 05-0661), respectively. These results suggest that TO comprising of Co−Ni−Cu contains the phases of Co_3O_4, NiO, and CuO, respectively.

3.2.2. FTIR Analysis. FT-IR spectroscopy, being an important tool for detecting the presence of hydroxyl ions and water molecules in the electrodeposited samples, was employed for the analysis of the TH and oxide materials. Figures 4 and 5 show the typical IR spectra of the THs and oxides, respectively. The presence of OH^- groups in Figure 4a implies that water molecules are associated as bound water within the crystal structure, which is as expected for hydroxide samples. For the sake of simplicity, only TH samples synthesized at optimized conditions from an electrolytic bath of 30 g dm^{-3} Co + 30 g dm^{-3} Ni + 10 g dm^{-3} Cu and its corresponding oxide form after calcination at 300 °C were selected, and the results were compared with the modified samples having surfactants CTAB and DTAB at the aforesaid optimized conditions. For all the samples studied, the strong

https://dx.doi.org/10.1021/acsomega.9b03657
ACS Omega 2020, 5, 3405−3417

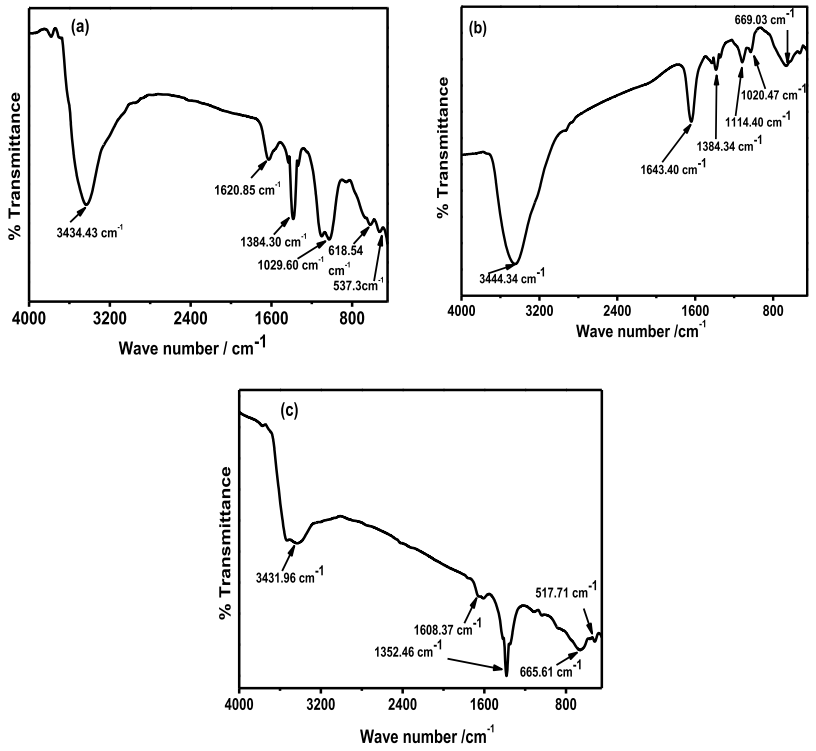

Figure 4. FT-IR spectra of ternary metal hydroxide (a) TH and modified ternary metal hydroxides with (b) $THCB_{CMC}$ and (c) $THDB_{CMC}$.

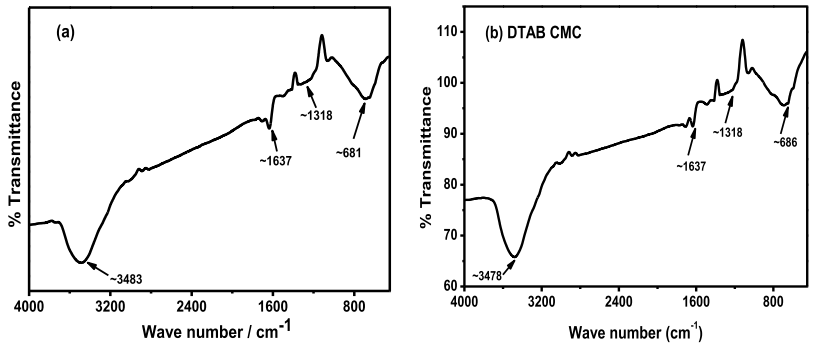

Figure 5. FT-IR spectra of the calcined form of ternary metal hydroxides (a) TO and modified ternary metal hydroxides with (b) $TODB_{CMC}$.

peak observed at 3400−3450 cm^{-1} are attributed to the stretching vibration of the O−H group of molecular water and hydrogen-bound O−H groups.[41−44] The weak band at the 1625 cm^{-1} region is due to the bending mode of water molecules.[45] The peak present between ∼500 and 600 cm^{-1} are described as Ni−O−H and/or Co−OH bending vibration.[46] The absorption band at 666 cm^{-1} can also be ascribed to Co−OH vibrations.[47] The spectrum also shows a peak at 1366.58 cm^{-1} indicating the presence of a Cu−OH bond,[48] and the peak at 881.41 cm^{-1} indicates Cu−OH vibrations,[49,50] indicating the hydroxide form of transition metal cations.

Figure 5 shows the FT-IR data of the calcined form of ternary metal hydroxides, which are TO and $TODB_{CMC}$. The peak positioned at 3483 and 1637 cm^{-1} for all the oxide samples are attributed to the adsorption of water on the surface of pellets because the FTIR sample were prepared in an ambient atmosphere.[51] The shoulder-like peak located at 1318 cm^{-1} is attributed to the interaction of the synthesized material with KBr.[51] The peak in the regions ∼500−700 cm^{-1} corresponds to the Co−O and Cu−O stretching vibration.[52] The absorption bands at 686 and 681 cm^{-1} are due to Co−O stretching vibration for the samples in the absence and presence of DTAB, respectively.[53]

3.2.3. Surface Morphology and EDS Analysis. The surface morphologies of the TO and modified TOs (TOCB, TODB) are shown in Figures 6−8. The SEM images show significant variation in the surface morphology and orientation of the crystals depending on the electrolytic bath in the absence and presence of surfactants and its micellar concentration. The nature and the concentration of the surfactant influence the microstructure of the electrodeposited product. Figure 6 shows the typical SEM images of TO at different magnifications with an energy-dispersive analysis data. The results revealed that TO showed a hierarchical architecture with microspheres within the range of 500 nm to 1 μm compactly arranged with no major detectable voids. However, the corresponding magnified image shows a porous nature of the material having tiny voids, with a natural sponge-like interconnected crystallite pores within the crystallite size of 100−200 nm. This will allow

https://dx.doi.org/10.1021/acsomega.9b03657
ACS Omega 2020, 5, 3405−3417

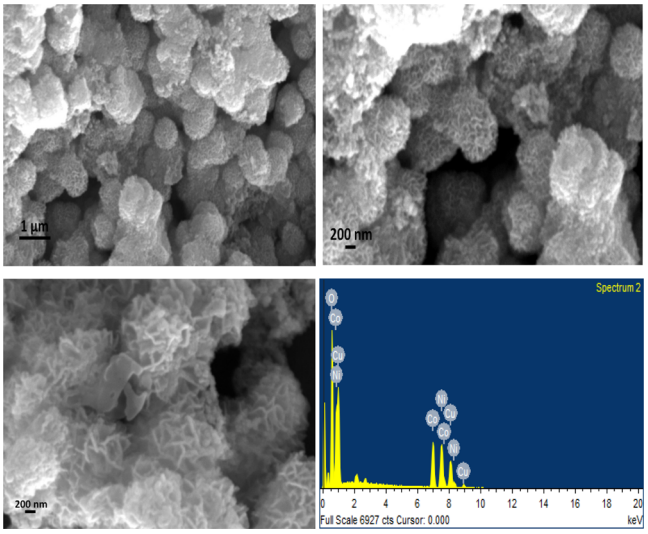

Figure 6. SEM images with EDS data of the calcined form of ternary metal hydroxides (TO) deposited from a nitrate bath containing 30 g dm^{-3} Co + 30 g dm^{-3} Ni and +10 g dm^{-3} Cu under different magnifications.

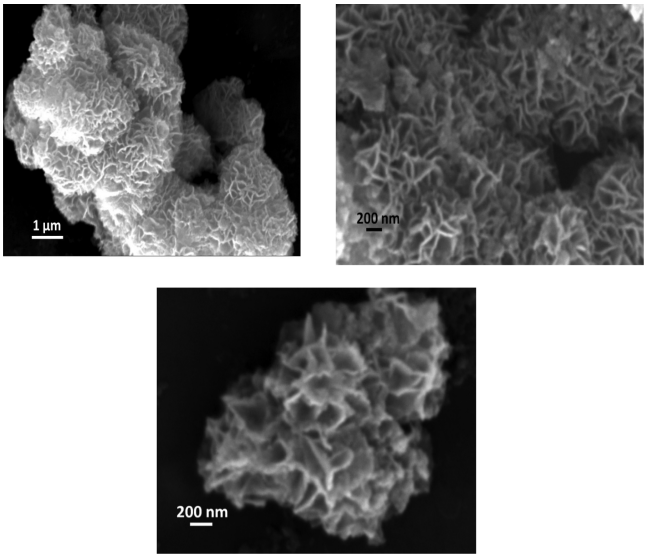

Figure 7. FESEM images of the modified ternary metal oxide $TOCB_{CMC}$ (different magnifications).

an easy penetration of ions from the electrolyte, facilitating the versatility of the material for storing energy reversibly. The relative intensities of the energy-dispersive spectral (EDS) analysis showed (in Table 2) that the TO material comprises of an approximately equal metal molar ratio of cobalt to nickel and copper ions present in the crystal lattice. The quantification of elements present at detectable concentrations represents 19, 17, and 8% for Co, Ni, and Cu, respectively.

The SEM image of $TOCB_{CMC}$ (Figure 7) exhibits a flower-like porous structure with an ununiform agglomeration of microspheres within the size ranging from 1 to 3 μm. At a higher magnification, the individual petals in the flower-shaped structure shows interconnected pores within the crystallite size ranging from 200 to 300 nm. A very similar results has also been observed for another surfactant DTAB, labelled $TODB_{LCMC}$ (shown in Figure 8a,b) and $TODB_{CMC}$ (Figure 8c,d) with a little variation of having a nanosheet-like

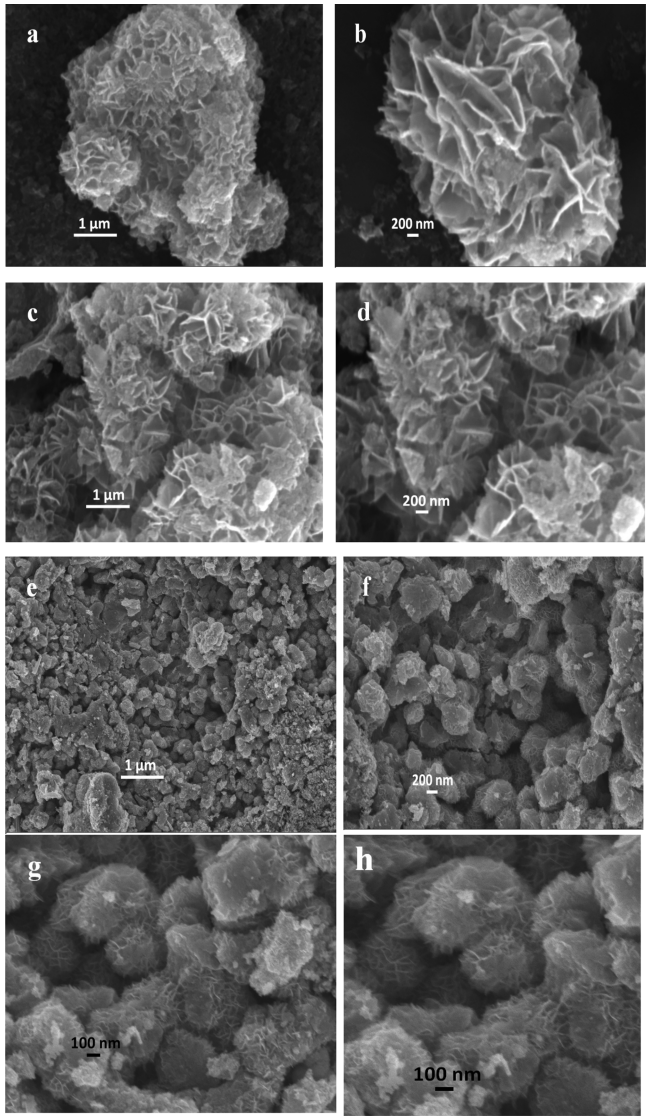

Figure 8. FESEM images of the modified ternary metal oxides (a,b) $TODB_{LCMC}$, (c,d) $TODB_{CMC}$, and (e–h) $TODB_{HCMC}$ (different magnifications).

Table 1. Atomic Absorption Spectrometer (AAS) Data of the TH Sample Obtained from 30 g dm^{-3} Co + 30 g dm^{-3} Ni with Variation of Cu in the Bath

sample (Co + Ni + Cu) g dm^{-3}	Co (%)	Ni (%)	Cu (%)
30 + 30 + 5	18.95	15.02	8.51
30 + 30 + 10	13.08	12.44	20.67
30 + 30 + 15	8.27	8.29	28.81

Table 2. AAS and EDS Data of the TO Sample TO at Optimized Condition

	composition (%)	
metal	AAS	EDS
Co	19.15	21.37
Ni	17.91	20.12
Cu	28.43	26.48

orientation and pore structure. $TODB_{LCMC}$ shows more bigger pores than $TODB_{CMC}$. However, in both the cases, pores are widely opened than those observed in the $TOCB_{CMC}$ sample

https://dx.doi.org/10.1021/acsomega.9b03657
ACS Omega 2020, 5, 3405–3417

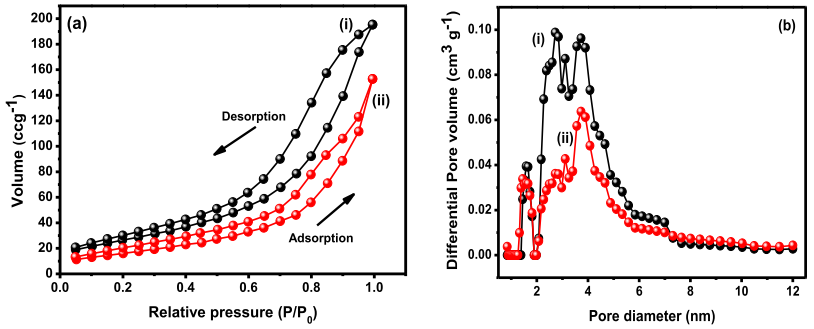

Figure 9. (a) Nitrogen adsorption−desorption and (b) pore-size distribution plots of (i) TO and (ii) $TODB_{HCMC}$ composites.

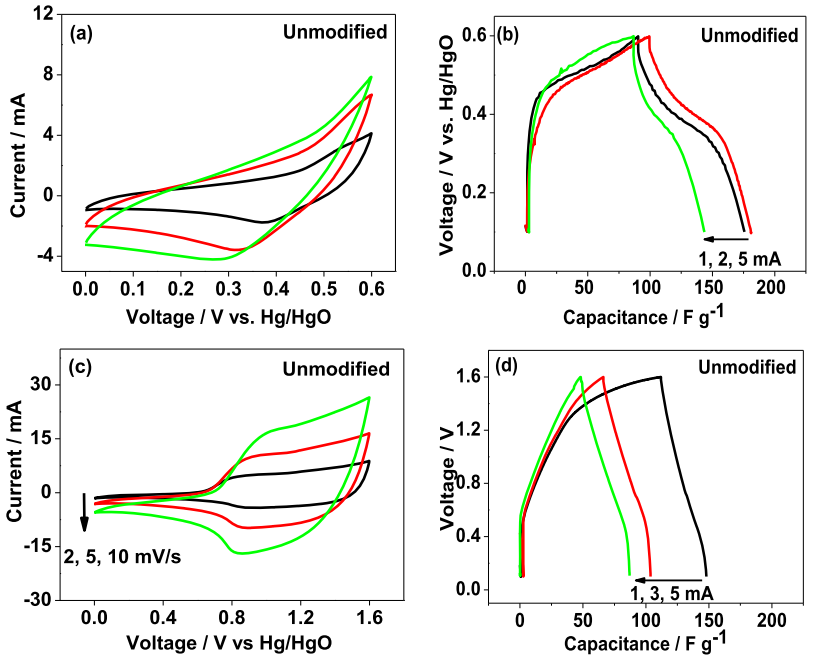

Figure 10. (a) Cyclic voltammetric (CV) curves and (b) charge−discharge behavior of ternary metal oxides (unmodified) in three-electrode configuration. Panels (c,d) are in two-electrode (hybrid cell) configuration. Sweep rates (mV/s) and charge−discharge current (mA) are shown in respective figures. The respective current densities are 0.03, 0.05, and 0.15 A/g.

(shown in Figure 7). The crystallite size is observed to decrease up to 100 nm or below in $TODB_{CMC}$, which increases the porosity in the material, resulting in better redox behavior of the material (discussed in the next section), supported by the porosity analysis in Section 3.2.4. Figure 8e−h shows the morphology of the $TODB_{HCMC}$ sample, where the higher concentration of the surfactant resulted in different particle shapes, more evenly distributed. At higher magnifications (Figure 8g,h), well-connected hierarchical nanospheres ranging from 200 to 400 nm are obtained with a less compact arrangement as compared to the TO sample (Figure 6), which may give more flexibility to the material to avail an easy transport of ions.

3.2.4. Porosity Analysis. To study the pore-size distribution of ternary metal oxides and modified TOs, nitrogen adsorption−desorption measurements were carried out. The adsorption−desorption isotherms and the corresponding Barrett−Joyner−Halenda (BJH) pore-size distribution curves of TO and the modified TO with the surfactant DTAB at high cmc ($TODB_{HCMC}$) are shown in Figure 9a,b. Both the samples corresponds to the type IV isotherm with a H2-type hysteresis loop, endorsing the meso porosity of the synthesized materials.[54] Sample TO showed the loop shifted to a higher relative pressure approaching P/P_0 = 0.99, suggesting the fact that the number of mesopores present is higher compared to that of $TODB_{HCMC}$. However, the loop of $TODB_{HCMC}$ at lower relative pressure may suggest the fact that the modified samples contain mesopores along with nanopores.

The BJH pore-size distribution curve showed a significant difference between TO and $TODB_{HCMC}$. Sample TO showed a narrow pore-size distribution curve with two peaks centered at about ∼3 and ∼4 nm; however, $TODB_{HCMC}$ showed an uniform broaden pore-size distribution curve with a peak centered at about ∼4 nm suggesting larger pore size with easy transfer of the electrolyte through the modified TO $TODB_{HCMC}$. This makes the electrode feasible to accommodate host ions on the surface of the material. The mixed nanopores and mesopores in $TODB_{HCMC}$ could reduce the diffusion distance for the electrolyte ion transport, increase the surface area, and enhance the adsorption of ions, making it an excellent material for the plausible electrochemical energy storage application.[55,56]

3.2.5. Chemical Analysis (AAS). Tables 1 and 2 compare the composition of the metals present in the sample Co + Ni + Cu

https://dx.doi.org/10.1021/acsomega.9b03657
ACS Omega 2020, 5, 3405−3417

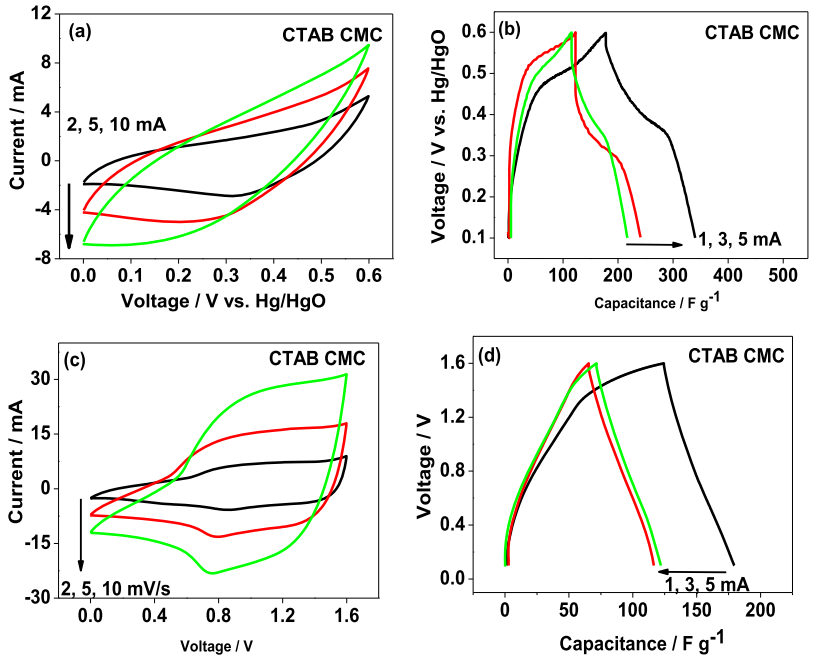

Figure 11. (a) Cyclic voltammetric (CV) curves and (b) charge−discharge behavior of modified ternary metal oxides (CTAB cmc) in three-electrode configuration. Panels (c,d) are in two-electrode (hybrid cell) configuration. Sweep rates (mV/s) and charge−discharge current (mA) are shown in respective figures. CTAB at a cmc is termed as "CTAB cmc". The respective current densities are 0.03, 0.05, and 0.15 A/g.

ternary metal hydroxides before (TH) and after (TO) calcination. The data were obtained by the wet chemical analysis of the electrodeposited sample using an atomic absorption spectrophotometer (AAS). The result revealed that with increasing copper concentration in the electrolytic nitrate bath, the percentage of copper in the uncalcined sample increases from 8.51 to 28.81% with a significant decrease in cobalt and nickel concentration. This may be due to more noble copper which get deposited/precipitated electrochemically faster than cobalt and nickel at it is in a favorable condition. Therefore, 10 g dm^{-3} Cu has been used throughout the studies. Table 2 shows the composition of TO synthesized after the calcination of TH obtained from the bath of 30 g dm^{-3}, Co +30 g dm^{-3}, and Ni +10 g dm^{-3} Cu, which showed that the composition of each metal increases after calcination.

3.3. Electrochemical Characterization. Apart from various metal oxides, carbon materials and conducting polymers are widely used in electrode fabrication for supercapacitors, the proposed ternary metal oxides present another alternative. The electrodes with poor electronic conductivity hamper the fast surface reaction at the interfaces, particularly for the pseudo-capacitors with redox-type reactions. Therefore, in the proposed ternary metal oxide, nickel and cobalt possess high electronic conductivity and redox behavior, while copper provides structural stability; consequently, ternary metal oxide is shown to enhance the electrochemical performance of the electrode. Additionally, the role of surfactants and the micelle concentrations on the energy storage is reported. Among the samples tested, $TODB_{HCMC}$ is shown to exhibit high specific capacitance and low resistance, making it viable to construct supercapacitors with high energy and power densities. To verify, ternary metal oxides in the absence and presence of surfactants and the micelle concentration have been investigated as promising electrode materials.

3.3.1. Ternary Metal Oxides. The electrochemical capacitance of the ternary metal oxide Co + Ni + Cu (optimal value of 30:30:10) was determined from cyclic voltammetry and galvanostatic (charge−discharge) studies carried out between 0.0 and 0.6 V (for three-electrode configuration) and 0.0−1.6 V (two electrode configuration) at a specified sweep rates indicated in the figure. The working electrode (ternary metal oxide) was cycled between 0.0 and 0.6 V at scan rates 2, 5, and 10 mV/s. On each cycle, the potential started at 0 V, moving initially in the anodic direction to 0.6 V and then subsequently, reversing it back to the original potential. Typically, 25 cycles have been performed to activate the material, and then the data have been collected.

Figure 10a displays the cyclic voltammetric (CV) profiles under the conditions noted in the figure. As can be seen in Figure 10a, the CV profile at a higher scan rate (10 mV/s) is well-defined consisting of a reduction peak at 0.3 V versus Hg/HgO region and a corresponding oxidation shoulder-like curve at a potential 0.5 V region. In a fixed potential window, the oxidation peaks would be incomplete for the curves scanned at higher sweep rates, implying the potential for this measurement is not sufficiently positive enough.[57] However, there is no clear indication of individual redox peaks to the respective cations (Co, Ni, and Cu), this could be due to their redox potentials being close to each other and inseparable.[57] The shape of the CV appears like a quasi-rectangular profile that exhibits near symmetry in shape, suggesting a pseudocapacitor behavior.[39] The corresponding charge−discharge curves (Figure 10b) show asymmetric (pseudocapacitive) behavior with near distortions, exhibiting a charge plateau at 0.5 V versus Hg/HgO and a discharge plateau-like curve at 0.3 V versus Hg/HgO, indicating that redox reactions occur.[58] The discharge specific capacitances of the ternary metal oxide corresponds to 185, 175, and 145 F/g at 1, 2 and 5 mA, respectively. The decrease in specific capacitance with an increasing current rate is due to the limited transfer of ions to

https://dx.doi.org/10.1021/acsomega.9b03657
ACS Omega 2020, 5, 3405−3417

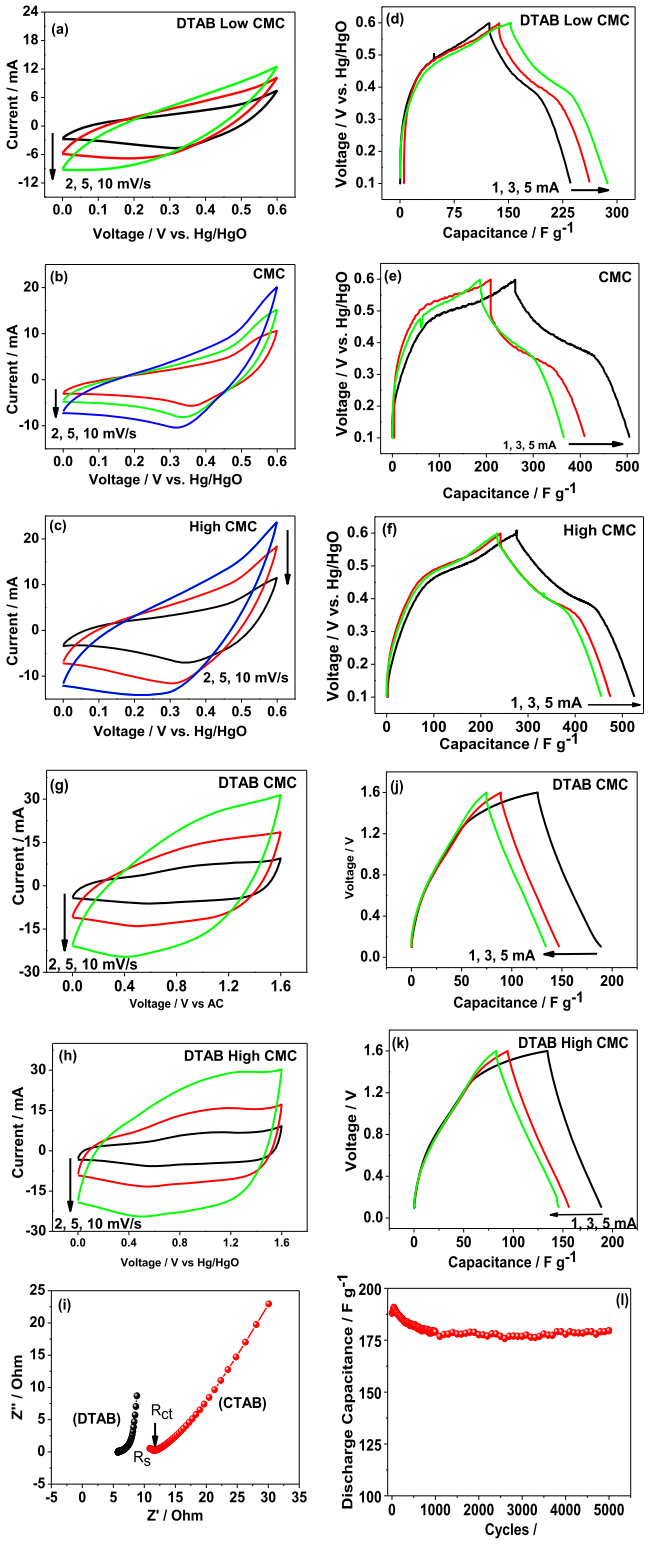

Figure 12. (a–c) Cyclic voltammetric (CV) curves and (d–f) charge–discharge behavior of modified ternary metal oxides (DTAB) in three-electrode configuration. (g,h,j,k) Two-electrode (hybrid cell—ac vs modified ternary metal oxides) configuration representing CV and CD, respectively. DTAB at three different concentrations is termed as DTAB cmc. Sweep rates (mV/s) and charge–discharge current (mA) are shown in respective figures. The respective current densities are 0.03, 0.05, and 0.15 A/g. (i) EIS spectra and (l) cycling stability of the hybrid cell—ac vs modified ternary metal oxides.

the pores, leading to unused pores of the electrode surface at 5 mA. However, the achieved high specific capacitance of 185 F/g is attributed to the porous nature of the microspheres with well interconnected crystallites (seen in Figure 6c SEM) attributed to the three metals that participated in the oxide. A hybrid device based on activated carbon as the capacitive negative electrode and ternary metal oxide as the pseudocapacitive positive electrode was made. The optimized potential window for the hybrid device was determined by measuring the suitable potential window for the positive electrode studied by three-electrode system in Figure 10a,b, which is 0.6 V. For the negative electrode (activated carbon) as reported by us earlier,[39] the operating voltage is 1.0 V, which is totally comprising 1.6 V. The CV curves (Figure 10c) exhibited a capacitor-like behavior while maintaining the shape with no distortion but the area under the curve (i.e. current response) increases on the higher sweep rates. In addition, the charge–discharge curves (Figure 10d) show a highly symmetric shape, suggesting a high reversibility. The hybrid device shows a specific capacitance of 145, 103, and 85 F/g at the discharge current of 1, 3, and 5 mA, respectively.

3.3.2. Modified Ternary Metal Oxides. To achieve one of another objectives, such as to enhance the faradaic reactions and attain better specific capacitance, ternary metal oxides in the presence of various surfactants with different micellar concentrations are tested. The presence of transition elements along with surfactants is expected to increase the capacitive behavior due to redox reactions. This is mainly because the obtained morphology for these samples is shown to play significant roles on the electrocapacitive performance of the electrodes.

The CV curves for the CTAB surfactant at the cmc level (shown in Figure 11a) indicate faradaic behavior within the voltage window tested, and the shape of the curves is like those of unmodified ternary metal oxide (in Figure 10a,b). However, the area under the curve is different, implying that more redox reaction occurred for the CTAB-modified sample. The corresponding charge–discharge curves (Figure 11b) show asymmetric (pseudocapacitive) behavior with near distortions and remain almost unchanged to that observed for the unmodified sample. Notably, the specific capacitance of the CTAB-modified sample delivered higher specific capacitance of 340, 235, and 210 mA h/g at a current density of 1, 3, and 5 mA, respectively. The obtained values are about two times higher than that of the performance shown in Figure 10. The modified ternary metal oxide presents a well-defined bent sheet-like structure grown in a random direction relating to the enhanced performance. A hybrid device performance constituting an activated carbon coupled with modified ternary metal oxide is shown in Figure 11c. The CV curves of the electrodes in Figure 11c show a potential of 1.6 V at sweep rates from 2 to 10 mV/s. It is found that the CV profiles are well maintained, indicating the high transport rate of electrons and its corresponding charge–discharge curves (Figure 11d) show 180, 122, 116 F/g at a current of 1, 3, and 5 mA revealing an excellent rate capability. The addition of CTAB amphiphilic surfactant composed of positively charged head and carbon tail acts as crystal growth modifiers[33,59] and their cmc level was vital for the formation of the obtained deposits.

To gain more insights, another cationic surfactant with a less hydrophobic chain, DTAB has been examined. A modified ternary metal oxide synthesized in the presence of a DTAB surfactant at three different micellar concentrations (below the

https://dx.doi.org/10.1021/acsomega.9b03657
ACS Omega 2020, 5, 3405–3417

Table 3. Summary of the Supercapacitor Materials with the Synthesis Techniques Employed and the Obtained Storage Performance with Reference to Our Current Work

		hybrid devices				
morphology	synthesis technique	electrolyte	electrode	specific capacitance	capacitance retention % (no. of cycles)	references
nano porous sea sponge Co−Ni oxide	galvanostatic electrodeposition	2 M NaOH	Co−Ni oxide//ac	76 F/g at 2 mA cm^{-2}	98% (1000)	39
flower-like $CuCo_2S_4/CuCo_2O_4$ heterostructure	hydrothermal	2 M KOH	$CuCo_2S_4/CuCo_2O_4$-4//graphene aerogel	37.5 F/g at 20 A/g	73% (10000)	65
$CuCo_2O_4$ maguey-like nanowires	hydrothermal	3 M KOH	symmetric device	982 F/g at 1.5 A/g	∼100 (1000)	66
corn-like $CuCo_2O_4$ nanoforest	hydrothermal	2 M KOH	symmetric device	820 F/g at 2 mA cm^{-2}	94% (1500)	67
nano cactus-like CuO−CoO core cell nanostructure	hydrothermal	3 M KOH	CuO−CoO//graphene ink	58.8 mA h g^{-1} at 1 A/g	86.5% (4000)	68
TOs of CoNiCu Porous microsphere	galvanostatic electrodeposition	2 M NaOH	$TODB_{HCMC}$//ac	188 F/g at 2 mA cm^{-2}	95.1 (1000)	this work

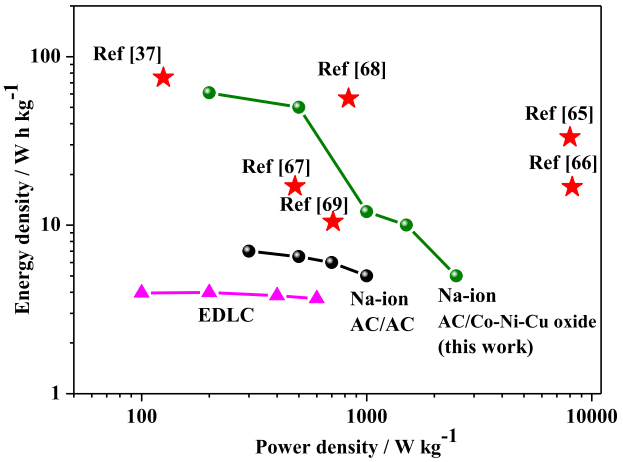

Figure 13. Ragone plot for various energy storage devices compared with the current work (hybrid cell—ac vs modified ternary metal oxides).

cmc, cmc, and above the cmc level) had been used as an electrode and tested in a three-cell configuration. Obviously, the CV curves for the DTAB high micellar concentration ($DTAB_{HCMC}$) showed a very well-defined peaks with larger integrated area becoming more prominent at higher sweep rates from 5 to 10 mV/s, as shown in Figure 12a−c. The corresponding symmetric shape of the charge−discharge without any distortions (Figure 12d−f) relates to a maximum specific capacitances 525, 475, 455 F/g at a discharge current of 1, 2, and 5 mA. Both the CV and CD curves (Figure 12a−f) clearly show that using DTAB as a surfactant improves the capacitance compared to the unmodified and CTAB surfactant material, with the high cmc addition (Figure 12c,f) achieving the maximum discharge capacitance. When an increasing amount of DTAB is used in the electrolytic bath during electrodeposition, the areas under the peaks are larger for the high cmc than the low cmc (Figure 12a,d) and cmc levels (Figure 12b,e). The higher amount of the surfactant may reduce the surface tension of the cathode during electrodeposition, which inhibits the formation of hydrogen in the bath and enhanced the quality of the ternary metal oxide deposits. This illustrates that the hierarchical nanosphere like the microstructure is formed (as shown in Figure 8) that can accelerate the electron transport and contribute to the formation of multiple active sites during the electrochemical reaction process, resulting in improved performance of energy storage. For hybrid device performance, activated carbon coupled with modified ternary metal oxide, remarkably, the integrated area of the CV curves (shown in Figure 12h,k) for the $DTAB_{HCMC}$ is larger and near rectangular in shape than that of $DTAB_{CMC}$, indicating a higher specific capacity for the former. This effect is clearly identified by increasing the amount of added DTAB in the bath which produces a better leveling effect at the electrodeposited surface. Moreover, the Nyquist plots for the modified TO material is shown in Figure 12i. The addition of DTAB in the modified oxide reduced the solution resistance (R_s) two times, not only that but also attained the smallest charge transfer resistance (R_{ct}) value of about 0.5 Ω. This result suggests that the $DTAB_{HCMC}$ material enhanced the electrical conductivity for the electrode, and R_{ct} is related to the unique hierarchical morphology of the oxide material. The charge−discharging behaviors of the modified TOs (Figure 12j,k) exhibit symmetrical and nearly linear characteristics, implying a capacitor nature. Indeed, the CV (Figure 12g,h) and CD (Figure 12j,k) curves (in a two-electrode system; hybrid cell) for $DTAB_{HCMC}$ further confirm that the voltage window of 1.6 V is safe and delivered a maximum capacitance of 188, 157, and 145 F/g at a current density of 0.03, 0.05, and 0.15 A/g. The hybrid device indicates 95.2% retention of the initial capacitance after 1000 cycles delivering 179 F/g, as shown in Figure 12l. Interestingly, after 5000 consecutive cycles, the capacitance retention remains 98% delivering 177 F/g. The role of Cu in the electrodeposited ternary metal oxide provides an excellent cycling stability of the electrode. However, an initial increase and then decrease in capacitance could be attributed to the activation process of the TO electrode during the initial cycles. The electrochemical performance of the ternary metal oxide reported in this work compares well and exceed the values to similar materials reported in the literature such as Co_3O_4 (57 F/g),[60] $NiCo_2O_4$ (64 F/g),[61] Co−Ni oxides (82 F/g),[62] $Ni_{0.8}Mn_{0.2}Fe_2O_4$ (147 F/g),[63] $NiMoO_4$ (100 F/g),[64] and other ternary metal oxides.[57] The obtained specific capacitance value (188 F/g at 0.1 A/g) for the modified ternary metal oxide exceeds the previously reported values for ternary metal oxide ZNCO[18] and MNCO.[32] This is shown to be attributed to the role of surfactants at the appropriate concentration. Furthermore, we have summarized the supercapacitor materials with the synthesis techniques employed, and the obtained storage performance has been compared with reference to our current work. The performances are shown in Table 3. Energy density and power density parameters are shown through the

https://dx.doi.org/10.1021/acsomega.9b03657
ACS Omega 2020, 5, 3405−3417

Ragone plot of the hybrid cell based on a two-electrode configuration in Figure 13. The performance data of the available capacitors in the market and few typical examples reported recently in the literature were also provided for comparison. The hybrid cell of the ternary metal oxide shows a maximum energy density of 61.6 W h/kg at 200 W/kg. With the power density increasing to 1500 W/kg, an energy density of 10 W h/kg can be maintained. These results confirm the electrochemical synthesis of ternary metal oxides and its role of surfactants and the CuO on the energy storage device. Overall, the obtained performance of this ternary metal oxide is higher than those of EDLC and Na-ion based symmetrical supercapacitors and comparable to that of asymmetrical supercapacitors previously reported.[37,65−69]

4. CONCLUSIONS

Facile synthesis of a ternary metal oxide, Co−Ni−Cu mixed oxide, is achieved by the electrodeposition/electrochemical precipitation technique using a diaphragm cell comprising a nitrate bath with a pH of ∼3 of the mixed electrolyte, followed by calcination at 300 °C. The in situ effect of two different surfactants CTAB and DTAB at various concentrations on the surface morphology, crystal structure, and the electrochemical performance of the synthesized materials for energy storage devices was investigated. The ternary metal oxide electrodes showed significant differences in the morphologies in the absence and presence of surfactants in the bath, which played a crucial role in determining the overall capacitive behaviors. The nitrogen adsorption desorption isotherm and pore size analysis provides strong evidence about the porous nature of the materials. The contributions of ternary metal oxide in the presence of a surfactant at a suitable micellar concentration on the electrocapacitive ability have never been discussed earlier. Among the samples studied, $DTAB_{HCMC}$ showed the maximum specific capacitance 188 F/g at a current density 0.1 A/g with a capacitance retention of 95% after 1000 cycles. The available capacitance was found to be stable thereafter until 5000 cycles. Choosing suitable metals and amount of surfactants to incorporate in the oxide through facile electrochemical synthesis is thus of a great importance to attain efficient energy storage with a high capacitance retention.

AUTHOR INFORMATION

Corresponding Author

Manickam Minakshi Sundaram − *College of Science, Health, Engineering & Education, Murdoch University, Perth, Western Australia 6150, Australia;* orcid.org/0000-0001-6558-8317; Phone: (+61) 08 9360 2017; Email: m.minakshi-sundaram@murdoch.edu.au

Authors

Avijit Biswal − *Department of Chemistry, College of Engineering & Technology (Autonomous), Bhubaneswar 751029, India*

Prasanna Kumar Panda − *CSIR-Institute of Minerals and Materials Technology, Bhubaneswar 751013, India*

Achyuta Nanda Acharya − *Department of Chemistry, College of Engineering & Technology (Autonomous), Bhubaneswar 751029, India*

Subhashree Mohapatra − *Department of Chemistry, College of Engineering & Technology (Autonomous), Bhubaneswar 751029, India*

Nibedita Swain − *Department of Chemistry, College of Engineering & Technology (Autonomous), Bhubaneswar 751029, India*

Bankim Chandra Tripathy − *CSIR-Institute of Minerals and Materials Technology, Bhubaneswar 751013, India*

Zhong-Tao Jiang − *College of Science, Health, Engineering & Education, Murdoch University, Perth, Western Australia 6150, Australia;* orcid.org/0000-0002-4221-6841

Complete contact information is available at: https://pubs.acs.org/10.1021/acsomega.9b03657

Notes

The authors declare no competing financial interest.

ACKNOWLEDGMENTS

Authors (A.B. and A.N.A.) would like to acknowledge the grant body, Technical Education Quality Improvement Program (TEQIP-III), Department of Higher Education, Government of India, for funding this work. One of the authors P.K.P. thanks Department of Science and Technology (DST), Govt. of India, for providing INSPIRE Fellowship to carry out doctoral research. M.M.S. would like to acknowledge the financial support from Murdoch University.

REFERENCES

(1) Burke, A. Ultracapacitors: Why, How, and Where Is the Technology. *J. Power Sources* **2000**, *91*, 37−50.

(2) Zhao, J.; Cheng, Y.; Yan, X.; Sun, D.; Zhu, F.; Xue, Q. Magnetic and electrochemical properties of $CuFe2_O4$ hollow fibers fabricated by simple electrospinning and direct annealing. *CrystEngComm* **2012**, *14*, 5879−5885.

(3) Miller, J. R.; Simon, P. Electrochemical Capacitors for *Energy Management. Sci. Magna* **2008**, *321*, 651−652.

(4) Jiang, H.; Lee, P. S.; Li, C. 3D Carbon Based Nanostructures for Advanced Supercapacitors. *Energy Environ. Sci.* **2013**, *6*, 41−53.

(5) Liu, B.; Liu, B.; Wang, Q.; Wang, X.; Xiang, Q.; Chen, D.; Shen, G. New Energy Storage Option: Toward $ZnCo_2O_4$ Nanorods/Nickel Foam Architectures for High-Performance Supercapacitors. *ACS Appl. Mater. Interfaces* **2013**, *5*, 10011−10017.

(6) Vialat, P.; Mousty, C.; Taviot-Gueho, C.; Renaudin, G.; Martinez, H.; Dupin, J.-C.; Elkaim, E.; Leroux, F. High-Performing Monometallic Cobalt Layered Double Hydroxide Supercapacitor with Defined Local Structure. *Adv. Funct. Mater.* **2014**, *24*, 4831−4842.

(7) Zhong, J.-H.; Wang, A.-L.; Li, G.-R.; Wang, J.-W.; Ou, Y.-N.; Tong, Y.-X. $Co_3O_4/Ni(OH)_2$ Composite Mesoporous Nanosheet Networks as a Promising Electrode for Supercapacitor Applications. *J. Mater. Chem.* **2012**, *22*, 5656−5665.

(8) Simon, P.; Gogotsi, Y. Materials for Electrochemical Capacitors. *Nat. Mater.* **2008**, *7*, 845−854.

(9) Wang, Q.; Liu, B.; Wang, X.; Ran, S.; Wang, L.; Chen, D.; Shen, G. Morphology evolution of urchin-like $NiCo_2O_4$ nanostructures and their applications as pseuuedocapacitors and photoelectrochemical cells. *J. Mater. Chem.* **2012**, *22*, 21647−21653.

(10) Wu, Z.-S.; Ren, W.; Wang, D.-W.; Li, F.; Liu, B.; Cheng, H.-M. High-energy MnO_2 Nanowire/graphene and Graphene Asymmetric Electrochemical Capacitors. *ACS Nano* **2010**, *4*, 5835−5842.

(11) Yan, J.; Fan, Z.; Sun, W.; Ning, G.; Wei, T.; Zhang, Q.; Zhang, R.; Zhi, L.; Wei, F. Advanced Asymmetric Supercapacitors Based on $Ni(OH)_2$/graphene and Porous Graphene Electrodes with High Energy Density. *Adv. Funct. Mater.* **2012**, *22*, 2632−2641.

(12) Lei, Z.; Christov, N.; Zhao, X. S. Intercalation of mesoporous carbon spheres between reduced graphene oxide sheets for preparing high-rate supercapacitor electrodes. *Energy Environ. Sci.* **2011**, *4*, 1866−1873.

(13) Chen, Z.; Qin, Y.; Weng, D.; Xiao, Q.; Peng, Y.; Wang, X.; Li, H.; Wei, F.; Lu, Y. Design and Synthesis of Hierarchical Nanowire

https://dx.doi.org/10.1021/acsomega.9b03657
ACS Omega 2020, 5, 3405−3417

Composites for Electrochemical Energy Storage. *Adv. Funct. Mater.* **2009**, *19*, 3420−3426.
(14) Dong, X.; Cao, Y.; Wang, J.; Chan-Park, M. B.; Wang, L.; Huang, W.; Chen, P. Hybrid structure of zinc oxide nanorods and three dimensional graphene foam for supercapacitor and electrochemical sensor applications. *RSC Adv.* **2012**, *2*, 4364−4369.
(15) Sarkar, D.; Khan, G. G.; Singh, A. K.; Mandal, K. High-Performance Pseudocapacitor Electrodes Based on α-Fe_2O_3/MnO_2 Core−Shell Nanowire Heterostructure Arrays. *J. Phys. Chem. C* **2013**, *117*, 15523−15531.
(16) Qu, Q.; Yang, S.; Feng, X. 2D Sandwich-like Sheets of Iron Oxide Grown on Graphene as High Energy Anode Material for Supercapacitors. *Adv. Mater.* **2011**, *23*, 5574−5580.
(17) Zhu, J.; He, J. Facile Synthesis of Graphene-Wrapped Honeycomb MnO_2 Nanospheres and Their Application in Supercapacitors. *ACS Appl. Mater. Interfaces* **2012**, *4*, 1770−1776.
(18) Wu, C.; Cai, J.; Zhang, Q.; Zhou, X.; Zhu, Y.; Shen, P. K.; Zhang, K. Hierarchical Mesoporous Zinc-Nickel-Cobalt Ternary Oxide Nanowire Arrays on Nickel Foam as High Performance Electrodes for Supercapacitors. *ACS Appl. Mater. Interfaces* **2015**, *7*, 26512−26521.
(19) Reddy, M. V.; Subba Rao, G. V.; Chowdari, B. V. R. Metal Oxides and Oxysalts as Anode Materials for Li Ion Batteries. *Chem. Rev.* **2013**, *113*, 5364−5457.
(20) Yuan, C.; Wu, H. B.; Xie, Y.; Lou, X. W. D. Mixed Transition-Metal Oxides: Design, Synthesis and Energy-Related Applications. *Angew. Chem., Int. Ed.* **2014**, *53*, 1488−1504.
(21) Zhang, Y.; Liu, Y.; Chen, J.; Guo, Q.; Wang, T.; Pang, H. Cobalt Vanadium Oxide Thin Nanoplates: Primary Electrochemical Capacitor Application. *Sci. Rep.* **2014**, *4*, 5687.
(22) Lee, M.-T.; Chang, J.-K.; Tsai, W.-T.; Lin, C.-K. In situ X-ray Absorption Spectroscopic Studies of Anodically Deposited Binary Mn−Fe Mixed Oxides with Relevance to Pseudocapacitance. *J. Power Sources* **2008**, *178*, 476−482.
(23) Lu, X.; Huang, X.; Xie, S.; Zhai, T.; Wang, C.; Zhang, P.; Yu, M.; Li, W.; Liang, C.; Tong, Y. *J. Mater. Chem.* **2012**, *22*, 13357−13364.
(24) Gomez, J.; Kalu, E. E.; Nelson, R.; Weatherspoon, M. H.; Zheng, J. P. Binder-Free Co−Mn Composite Oxide for Li−Air Battery Electrode. *J. Mater. Chem. A* **2013**, *1*, 3287−3294.
(25) Zhou, L.; Zhao, D.; Lou, X. W. Double-shelled $CoMn_2O_4$ Hollow Microcubes as High-Capacity Anodes for Lithium- Ion Batteries. *Adv. Mater.* **2012**, *24*, 745−748.
(26) Wei, T.-Y.; Chen, C.-H.; Chien, H.-C.; Lu, S.-Y.; Hu, C.-C. A Cost-Effective Supercapacitor Material of Ultrahigh Specific Capacitances: Spinel Nickel Cobaltite Aerogels from an Epoxide-Driven Sol-Gel Process. *Adv. Mater.* **2010**, *22*, 347−351.
(27) Zhang, G.; Yu, L.; Wu, H. B.; Hoster, H. E.; Lou, X. W. D. Formation of $ZnMn_2O_4$ Ball-in-Ball Hollow Microspheres as a High-Performance Anode for Lithium-ion Batteries. *Adv. Mater.* **2012**, *24*, 4609−4613.
(28) Wang, X.; Yan, C.; Sumboja, A.; Lee, P. S. High Performance Porous Nickel Cobalt Oxide Nanowires for Asymmetric Supercapacitor. *Nano Energy* **2014**, *3*, 119−126.
(29) Zhang, J.; Cheng, J. P.; Li, M.; Liu, L.; Liu, F.; Zhang, X. B. Flower-Like Nickel−Cobalt Binary Hydroxides with High Specific Capacitance: Tuning the Composition and Asymmetric Capacitor Application. *J. Electroanal. Chem.* **2015**, *743*, 38−45.
(30) Patil, U. M.; Sohn, J. S.; Kulkarni, S. B.; Lee, S. C.; Park, H. G.; Gurav, K. V.; Kim, J. H.; Jun, S. C. Enhanced Supercapacitive Performance of Chemically Grown Cobalt- Nickel Hydroxides on Three-Dimensional Graphene Foam Electrodes. *ACS Appl. Mater. Interfaces* **2014**, *6*, 2450−2458.
(31) Luo, J.-M.; Gao, B.; Zhang, X.-G. High Capacitive Performance of Nanostructured Mn-Ni-Co Oxide Composites for Supercapacitor. *Mater. Res. Bull.* **2008**, *43*, 1119−1125.
(32) Li, L.; Zhang, Y.; Shi, F.; Zhang, Y.; Zhang, J.; Gu, C.; Wang, X.; Tu, J. Spinel Manganese- Nickel-Cobalt Ternary Oxide Nanowire Array for High-Performance Electrochemical Capacitor Applications. *ACS Appl. Mater. Interfaces* **2014**, *6*, 18040−18047.
(33) Zhang, H.; Wang, Y.; Liu, C.; Jiang, H. Influence of surfactant CTAB on the electrochemical performance of manganese dioxide used as supercapacitor electrode material. *J. Alloys Compd.* **2012**, *517*, 1−8.
(34) Li, Y.; Cai, X.; Shen, W. Preparation and performance comparison of supercapacitors based on nanocomposites of MnO_2 with cationic surfactant of CTAC or CTAB by direct electrodeposition. *Electrochim. Acta* **2014**, *149*, 306−315.
(35) Zhang, H.; Gu, J.; Jiang, Y.; Wang, Y.; Zhao, J.; Zhang, X.; Wang, C. Calcination removing soft template cetyl trimethyl ammonium bromide and its effects on capacitance performance of supercapacitor electrode MnO_2. *Energy Convers. Manage.* **2014**, *86*, 605−613.
(36) Biswal, A.; Tripathy, B. C.; Subbaiah, T.; Meyrick, D.; Minakshi, M. Electrodeposition of manganese dioxide: effect of quaternary amines. *J. Solid State Electrochem.* **2013**, *17*, 1349−1356.
(37) Lee, H.-M.; Cho, S.-W.; Song, C.-J.; Kang, H. J.; Kwon, B. J.; Kim, C.-K. Abrupt change with surfactant concentration in the surface morphology of the electrodeposited manganese oxide films for electrochemical capacitors. *Electrochim. Acta* **2015**, *160*, 50−56.
(38) Biswal, A.; Tripathy, B. C.; Subbaiah, T.; Meyrick, D.; Minakshi, M. Dual Effect of Anionic Surfactants in the Electrodeposited MnO_2Trafficking Redox Ions for Energy Storage. *J. Electrochem. Soc.* **2015**, *162*, A30−A38.
(39) Biswal, A.; Panda, P.; Jiang, Z.-T.; Tripathy, B.; Minakshi, M. Facile synthesis of a nanoporous sea sponge architecture in a binary metal oxide. *Nanoscale Adv.* **2019**, *1*, 1880−1892.
(40) Brownson, J. R. S.; Lévy-Clément, C. Electrodeposition of α- and β-cobalt hydroxide thin films via dilute nitrate solution reduction. *Phys. Status Solidi B* **2008**, *245*, 1785−1791.
(41) Su, L.-H.; Zhang, X.-G.; Mi, C.-H.; Gao, B.; Liu, Y. Improvement of the capacitive performances for Co−Al layered double hydroxide by adding hexacyanoferrate into the electrolyte. *Phys. Chem. Chem. Phys.* **2009**, *11*, 2195−2202.
(42) Villegas, J. C.; Giraldo, O. H.; Laubernds, K.; Suib, S. L. New Layered Double Hydroxides Containing Intercalated Manganese Oxide Species: Synthesis and Characterization. *Inorg. Chem.* **2003**, *42*, 5621−5631.
(43) Xu, R.; Zeng, H. C. Mechanistic Investigation on Salt-Mediated Formation of Free-Standing Co_3O_4 Nanocubes at 95 °C. *J. Phys. Chem. B* **2003**, *107*, 926−930.
(44) Khan, Y.; Durrani, S. K.; Mehmood, M.; Jan, A.; Abbasi, M. A. pH-dependant structural and morphology evolution of $Ni(OH)_2$ nanostructures and their morphology retention upon thermal annealing to NiO. *Mater. Chem. Phys.* **2011**, *130*, 1169−1174.
(45) Frost, R. L.; Kloprogge, J. T. Infrared emission spectroscopic study of brucite. *Spectrochim. Acta, Part A* **1999**, *55*, 2195−2205.
(46) Xie, L.; Song, H.; Wang, Y.; Xu, W.; Bai, X.; Dong, B. Influence of Concentration Effect and Au Coating on Photoluminescence Properties of YVO_4: Eu^{3+} Nanoparticle Colloids. *J. Phys. Chem. C* **2010**, *114*, 9975−9980.
(47) Barauskienė, I.; Valatka, E. Synthesis, structure and capacitive properties of cobalt hydroxide films on stainless steel substrates. *Cent. Eur. J. Chem.* **2014**, *12*, 1206−1211.
(48) Rath, R. K.; Subramanian, S.; Sivanandam, V.; Pradeep, T. Studies on the interaction of Guar gum with Chalcopyrite. *Can. Metall. Q.* **2001**, *40*, 1−11.
(49) Aguirre, J. M.; Adamo, G.; Oscar, G. Simple route for the synthesis of copper hydroxy salts. *J. Braz. Chem. Soc.* **2011**, *22*, 546−551.
(50) Henrist, C.; Mathieu, J.-P.; Vogels, C.; Rulmont, A.; Cloots, R. Morphological study of magnesium hydroxide nanoparticles precipitated in dilute aqueous solution. *J. Cryst. Growth* **2003**, *249*, 321−330.
(51) Taşköprü, T.; Zor, M.; Turan, E. Structural characterization of nickel oxide/hydroxide nanosheets produced by CBD technique. *Mater. Res. Bull.* **2015**, *70*, 633−639.

https://dx.doi.org/10.1021/acsomega.9b03657
ACS Omega 2020, 5, 3405−3417

(52) Yuan, G.-Q.; Jiang, H.-F.; Lin, C.; Liao, S.-J. Shape-and Size-Controlled Electrochemical Synthesis of Cupric Oxide Nanocrystals. *J. Cryst. Growth* **2007**, *303*, 400−406.
(53) Zhou, L.; Xu, J.; Miao, H.; Wang, F.; Li, X. Catalytic oxidation of cyclohexane to cyclohexanol and cyclohexanone over Co3O4 nanocrystals with molecular oxygen. *Appl. Catal., A* **2005**, *292*, 223−228.
(54) Aranovich, G.; Donohue, M. Analysis of adsorption isotherms: lattice theory predictions, classifications of isotherms for gas-solid equilibria, and similarities in gas and liquid adsorption behaviour. *J. Colloid Interface Sci.* **1998**, *200*, 273−290.
(55) Dong, D.; Liu, Y.; Li, J. Co_3O_4 hollow polyhedrons as bifunctional electrocatalysts for reduction and evolution reactions of oxygen. *Part. Part. Syst. Char.* **2016**, *33*, 887−895.
(56) Wu, Z.; Li, L.; Yan, J.-m.; Zhang, X.-b. Materials Design and System Construction for Conventional and New Concept Supercapacitors. *Adv. Sci.* **2017**, *4*, 1600382.
(57) Huang, Y.-Y.; Lin, L.-Y. Synthesis of ternary metal oxides for battery-supercapacitor devices: influences of metal species on redox reaction and electrical conductivity. *ACS Energy Mater.* **2018**, *1*, 2979−2990.
(58) Zhao, D.; Dai, M.; Tong, Y.; Song, X.; Wu, X. Mixed transition metal oxide nanowire arrays enabling hybrid capacitor performance enhancement. *CrystEngComm* **2019**, *21*, 5789−5796.
(59) Mohanty, U. S.; Tripathy, B. C.; Singh, P.; Keshavarz, A.; Iglauer, S. Roles of organic and inorganic additives on the surface quality, morphology, and polarization behaviour during nickel electrodeposition from various baths: a review. *J. Appl. Electrochem.* **2019**, *49*, 847−870.
(60) Liu, W.; Li, X.; Zhu, M.; He, X. High-performance all-solid state asymmetric supercapacitor based on Co_3O_4 nanowires and carbon aerogel. *J. Power Sources* **2015**, *282*, 179−186.
(61) Zhu, J.; Jiang, J.; Sun, Z.; Luo, J.; Fan, Z.; Huang, X.; Zhang, H.; Yu, T. 3D Carbon/Cobalt-Nickel Mixed-Oxide Hybrid Nanostructured Arrays for Asymmetric Supercapacitors. *Small* **2014**, *10*, 2937−2945.
(62) Zhang, J.; Liu, F.; Cheng, J. P.; Zhang, X. B. Binary Nickel-cobalt Oxides Electrode Materials for High-performance Supercapacitors: Influence of its Composition and Porous Nature. *ACS Appl. Mater. Interfaces* **2015**, *7*, 17630−17640.
(63) Zate, M. K.; Shaikh, S. M. F.; Jadhav, V. V.; Tehare, K. K.; Kolekar, S. S.; Mane, R. S.; Naushad, M.; Pawar, B. N.; Hui, K. N. Synthesis and Electrochemical Supercapacitive Performance of Nickel−Manganese Ferrite Composite Films. *J. Anal. Appl. Pyrolysis* **2015**, *116*, 177−182.
(64) Chen, T.; Shi, R.; Zhang, Y.; Wang, Z. A $MnCo_2O_4$@$NiMoO_4$ Core-Shell Composite Supported on Nickel Foam as a Supercapacitor Electrode for Energy Storage. *ChemPlusChem* **2019**, *84*, 69−77.
(65) Xu, X.; Liu, Y.; Dong, P.; Ajayan, P. M.; Shen, J.; Ye, M. Mesostructured $CuCo_2S_4$/$CuCo_2O_4$ nanoflowers as advanced electrodes for asymmetric supercapacitors. *J. Power Sources* **2018**, *400*, 96−103.
(66) Liao, L.; Zhang, H.; Li, W.; Huang, X.; Xiao, Z.; Xu, K.; Yang, J.; Zou, R.; Hu, J. Facile synthesis of maguey-like $CuCo_2O_4$ nanowires with high areal capacitance for supercapacitors. *J. Alloys Compd.* **2017**, *695*, 3503−3510.
(67) Wang, Y.; Yang, D.; Lian, J.; Wei, T.; Sun, Y. Ordered corn-like $CuCo_2O_4$ nanoforests covering Ni foam for a high-performance all-solid-state supercapacitor. *J. Alloys Compd.* **2018**, *741*, 527−531.
(68) Gopi, C. V. V. M.; Vinodh, R.; Sambasivam, S.; Obaidat, I. M.; Naidu Kalla, R. M.; Kim, H.-J. One-pot synthesis of copper oxide−cobalt oxide core−shell nanocactus-like heterostructures as binder-free electrode materials for high-rate hybrid supercapacitors. *Mater. Today Energy* **2019**, *14*, 100358.
(69) Xu, H.; Hu, X.; Yang, H.; Sun, Y.; Hu, C.; Huang, Y. Flexible asymmetric micro-supercapacitors based on Bi_2O_3 and MnO_2 nanoflowers: Larger areal mass promises higher energy density. *Adv. Energy Mater.* **2015**, *5*, 1401882.

https://dx.doi.org/10.1021/acsomega.9b03657
ACS Omega 2020, 5, 3405−3417